Kovove Mater. 62 2024 91–100
DOI: 10.31577/km.2024.2.91

Influence of tool rotational speed on the microstructure and mechanical behavior of friction stir processed AA 7050 aluminum alloy

Ali Debih[1]*, Hiba Azzeddine[2]

[1] *Faculty of Technology, Mechanical Department, University of M'sila, 28000 M'sila, Algeria*
[2] *Laboratory of Materials and Renewable Energy, Faculty of Sciences, Mohamed Boudiaf University, 28000 M'sila, Algeria*

Received 21 November 2023, received in revised form 13 Februar 2024, accepted 10 April 2024

Abstract

The present study investigated the effect of tool rotational speed on the microstructure and mechanical behavior of friction stir processed AA 7050 aluminum alloy using an optical micrograph, scanning electron microscope, tensile test, impact strength, and Vickers microhardness. The alloy was processed at 40 mm min^{-1} as a travel speed combined with three tool rotational speeds, 800, 1200, and 1600 rpm. The visual inspection of the surfaces of the samples revealed that the alloy could be successfully friction stir processed at any rotational speed. The results indicated that the mean grain size of the stir zone decreases with increasing the tool rotational speed (from 45 to 9 μm). The development of the precipitates θ, (η' and η), (T′ and T), and S′ phases was significantly controlled by the tool rotational speed. Consequently, the microhardness, tensile strength, and impact strength of the AA7050 alloy were enhanced by friction stir processing due to the combination of grain refinement and precipitation strengthening. The optimum mechanical properties were obtained for the sample processed with a tool rotational speed of 1600 rpm.

K e y w o r d s: friction stir processing, 7050 aluminum alloy, tensile properties, hardness, impact

1. Introduction

Aluminum alloys such as the 7xxx series (Al-Zn--Mg-Cu) are widely used for fabricating high-strength and lightweight structures in electrical engineering, aerospace, and automotive industries owing to their high strength-to-weight ratio, high conductivity, and good corrosion resistance [1, 2].

It is well known that improving the alloy's performance can be achieved by grain refinement through the Hall-Petch relation [3, 4]. Severe plastic deformation (SPD) processing is now considered the most effective procedure for producing materials with ultrafine-grained (UFG) microstructures [5]. In addition, it was demonstrated that SPD processing could significantly alter the precipitation sequence and the age-hardening response of UFG materials due to the introduction of a high number of defects, such as dislocations, grain boundaries, and vacancies that play preferential sites of precipitate nucleation [6, 7]. Consequently, the mechanical properties of the SPD--processed materials can be further controlled by the combination of strengthening from grain refinement and precipitation hardening.

Today, several SPD processing techniques are available, such as equal channel angular processing (ECAP) [8], accumulative roll bonding (ARB) [9], high-pressure torsion (HPT) [10], and friction stir processing (FSP) [11]. FSP is a solid-state process for material consolidation derived from friction stir welding (FSW) [12]. FSW is a pioneering welding process that can join aluminum-based alloys, which are usually extremely difficult to weld using traditional techniques like fusion welding or arc welding [2].

FSP can produce UFG microstructure in a single pass using a non-consumable rotating tool with a shoulder and pin traversing along a specific workpiece region, as illustrated in Fig. 1 [13]. Friction between

*Corresponding author: e-mail address: ali.debih@univ-msila.dz

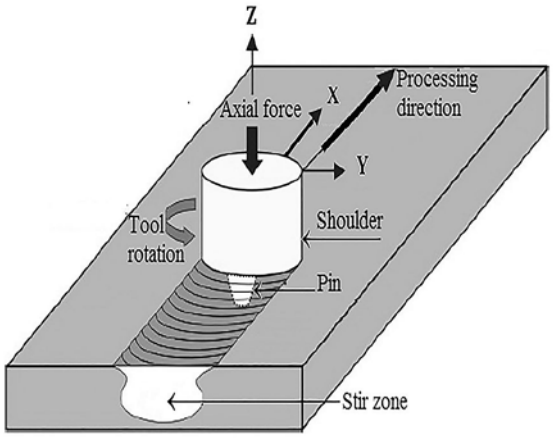

Fig. 1. An illustration showing the friction stir processing.

the tool shoulder and the workpiece results in severe plastic deformation introduced by the high-speed stir tool and localized heating generated by the rotating tool and the workpiece that softens and plasticizes the processed zone, which eventually produces an ultrafine grain structure with high-angle grain boundaries [11, 13, 14]. However, a complex microstructure is often reported in the FSP materials, and it can be separated into four distinct regions: (1) stir zone (SZ), (2) thermomechanically affected zone (TMAZ), (3) heat affected zone (HAZ), and (4) base metal (BM) [13].

The literature includes research by various researchers on the evolution of the microstructure and mechanical behavior of aluminum-based alloys after FSP [15–22]. These investigations have demonstrated that FSP parameters such as tool geometry, tool rotation speed, and travel speed influence the microstructure and corresponding mechanical properties.

However, further research efforts are still needed to optimize the FSP parameters and extend our knowledge of controlling the design and manufacture of aluminum-based alloys for different industrial applications. Hence, the present study aims to explore the effect of tool rotational speed on the microstructural characteristics of the stir zone of the AA7050 alloy after FSP. In addition, the mechanical performances were evaluated as a function of rotational speed using the tensile test, impact strength, and Vickers microhardness measurements.

2. Experimental procedure

An industrial rolled plate of AA7050 alloy was slashed into the required form of a rectangular plate of $200 \times 120\,\text{mm}^2$ and 5 mm in thickness. The chemical composition of the alloy, as determined by emission spectroscopy by ASTM B247, is shown in Table 1.

The friction stir processing was performed using

Table 1. Chemical composition in weight percentage (wt.%) of the as-received AA7050 alloy

Cu	Zn	Mg	Zr	Fe	Si	Mn
2.3	6.2	6	0.12	0.08	0.1	0.09

Fig. 2. (a) Cylindrical pin FSP tool, (b) FSP experimental setup, and (c) sampling direction cut for the tensile tests.

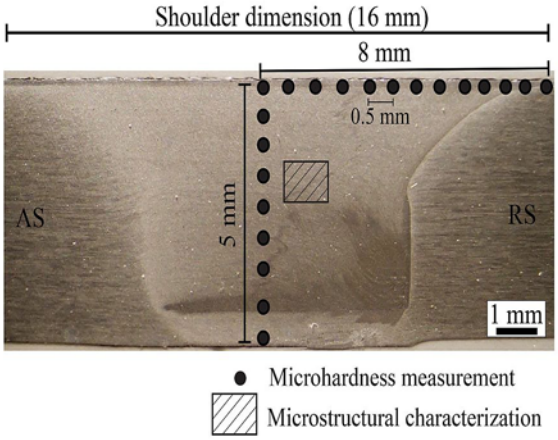

Fig. 3. Optical micrograph of the longitudinal cross-section of Al 7050 alloy after FSP and the microstructural and microhardness measurements positions. AS and RS mean advancing and retreating sides, respectively.

a non-consumable tool with a cylindrical pin made from high-speed steel (HSS-Co5). As shown in Fig. 2a, the tool has a shoulder diameter, pin diameter, and pin length of 16, 5, and 4 mm, respectively. The experimentation was carried out on equipment consisting of a modified vertical milling machine (HURON), as demonstrated in Fig. 2b, in which the fixture was made to ensure rigid clamping of the plates during the processing.

The cinematic parameters of FSP for the AA 7050 alloy were fixed at a constant speed of 40 mm min^{-1} and different rotation speeds: 800, 1200, and 1600 rpm. FSP was performed several times by moving in 20 mm increments toward the advancing side.

Figure 3c shows the sample cutting preparation for the tensile test. The processed plates were cut using an electro-discharge machine according to the ASTM B557M-14 specifications with dimensions of a gauge length of 25 mm, a thickness of 5 mm, and a gauge width of 6 mm. Tensile tests were performed on each sample until the failure was achieved using a hydraulic testing machine at room temperature and a strain rate of 10^{-3} s^{-1}. Three samples were tested for each rotational speed condition, and the average data was presented.

Impact strength tests were conducted at room temperature using an impact testing machine type (Instron Wolpert) with a maximum capacity of 300 J. Under-sized Charpy impact V-notch test specimens of $55 \times 10 \times 5$ mm^3 were cut from the plates. At least three samples were tested for each rotational speed condition, and the average value was presented.

The microhardness profile was measured along the cross-section of the stir zone, from the top to the bottom and from the center to the outside line of the stir zone, as shown in Fig. 3. The microhardness measurements were carried out using a Vickers microhardness tester type (TUKON 2500) with a 0.5 N load and a dwell time of 15 s.

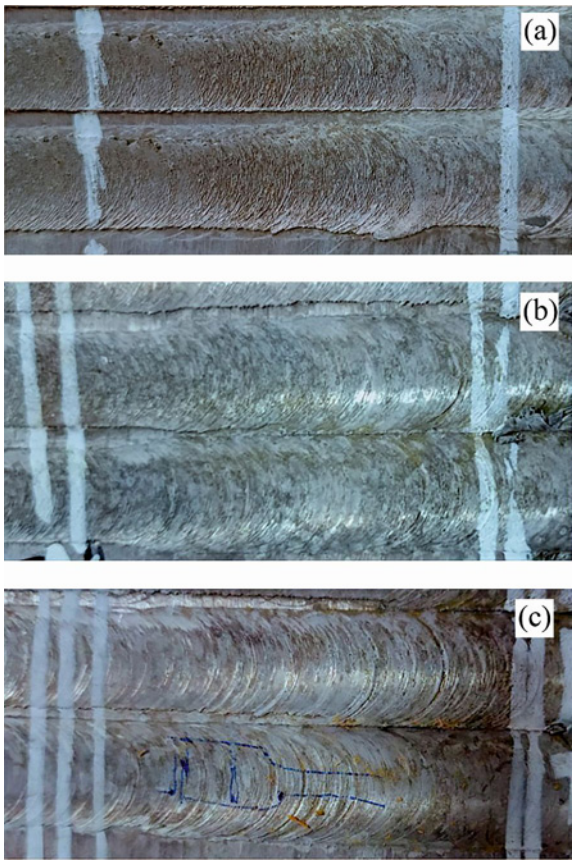

Fig. 4. Top surface morphologies of the processed zone at rotation speeds of (a) 800, (b) 1200, and (c) 1600 rpm.

The stir zones of the processed samples were subjected to microstructural observations using an optical metallographic microscope, as illustrated in Fig. 3. The stirred surfaces were first polished and then etched using Keller's reagent: 190 ml H_2O, 5 ml HNO_3, 3 ml HCl, and 2 ml HF.

Additional microstructural observations and structural investigations were jointly performed by a scanning electron microscope (SEM) combined with energy dispersive X-ray (EDX) analyses.

X-ray diffraction (XRD) patterns were recorded using an X'PERT PRO MPD diffractometer operating at a voltage of 35 kV and a current of 40 mA, using Cu-Kα (1.5418Å) radiation. The data were collected over a range of $2\theta = 30°$–$90°$ with a scanning step of 0.02°.

3. Results and discussion

3.1. Microstructural evolution

Figure 4 illustrates the surface of the stirring AA 7050 aluminum alloy after processing at 800, 1200,

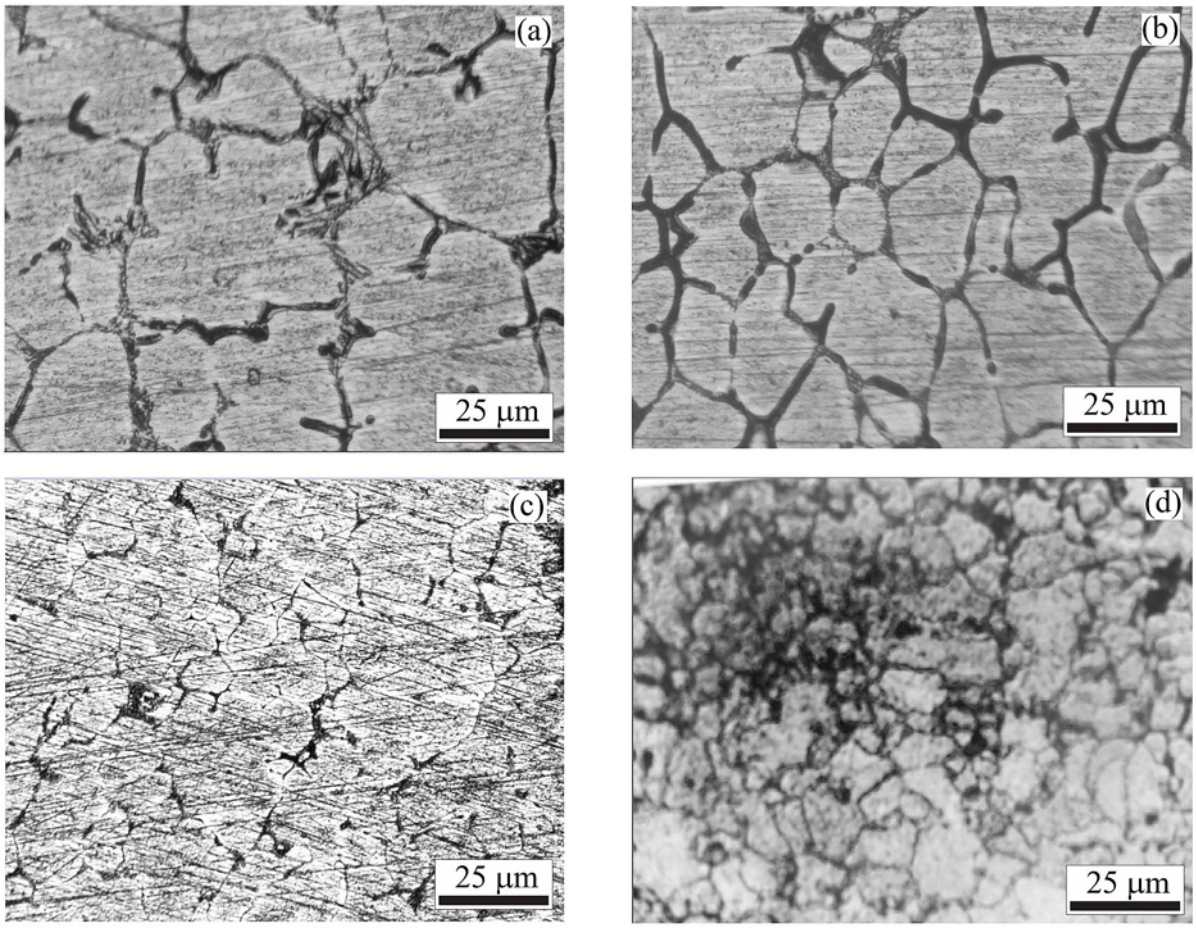

Fig. 5. Optical micrographs of (a) unprocessed alloy and stirred zone at rotational speeds of (b) 800, (c) 1200, and (d) 1600 rpm.

and 1600 rpm. The visual analyses of the processed surfaces show that the surface areas of the stirred zones are uniformly mixed without any cracks or defects. However, the surface quality is dependent on the tool rotational speed parameter. It can be seen from Figs. 4a,b that the surface appearance is less smooth at low rotation speeds (800 and 1200 rpm).

The roughness fluctuation in the stirred surfaces is due to the variation in heating amount generated during stirring caused by the rotation speed level. By reducing the tool rotation speed from 1600 to 800 rpm, the heat generated during stirring increases the plasticity of the material. It can be observed that the internal resistance of the material increases due to the reduction in the particle size of the stirred zones in the material, which results in an improvement in the roughness of the surfaces as a function of the rotation speed.

Figure 5 presents the microstructure of the unprocessed sample and the stir zones of the FSP samples at 800, 1200, and 1600 rpm. As shown in Fig. 5a, the as-received sample comprises globular grains with a mean grain size of 45 μm and intermetallic phases in the form of dendrites along the grain boundaries. The microstructure of the stir zone at 800 rpm is very similar to the unprocessed sample, except that the mean grain size seems smaller (about 28 μm). The amount of deformation and the heat generated at 800 rpm seem insufficient to change the dendritic microstructure of the alloy. While increasing rotational speed from 1200 to 1600 rpm results in visible grain refinement, the mean grain size reached a value of 9 μm at the rotational speed of 1600 rpm (Fig. 5d). The development of fine microstructure in the stir zone is attributed to the occurrence of dynamic recrystallization (DRX). The combination of severe plastic deformation and heating during stirring allowed the accumulation of dislocations, leading to low-angle grain boundaries and their transformation into high-angle grain boundaries [23]. Figure 5 shows that the distribution of intermetallic phases along the grain boundaries significantly changes with increasing rotational speed.

SEM micrographs and EDS analysis shown in Fig. 6 and Table 2 were used to identify the intermetallic phases present in the unprocessed sample and the stir zone of the processed samples at 800, 1200, and

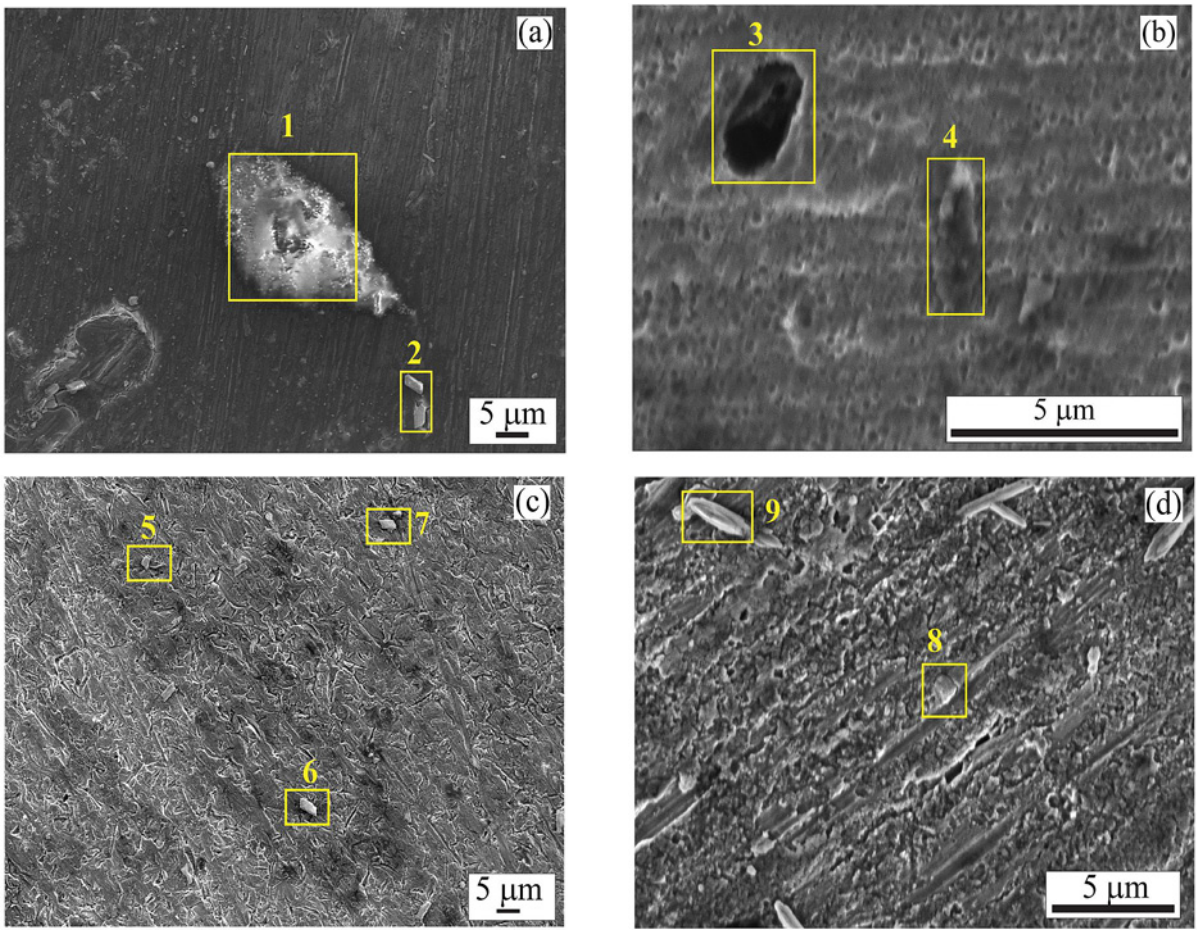

Fig. 6. SEM micrographs of (a) unprocessed alloy and stirred zone at rotational speeds of (b) 800, (c) 1200, and (d) 1600 rpm.

Table 2. EDS analysis in atomic percentage (at. %) of phases present in the unprocessed and processed samples at 800, 1200, and 1600 rpm

Condition	Spot	Al	Mg	Cu	Zn	Si	Mn	O	Fe	Possible phase
Unprocessed alloy	1	21.91	64.26	1.93	11.18	0.34	0.27	0.11	–	T-$(AlZn)_{49}Mg_{32}$
	2	50.72	–	48.97	–	0.22	–	–	0.09	θ-Al_2Cu
FSP at 800 rpm	3	–	5.33	1.28	93.31	–	0.08	–	–	η'-Mg_2Zn_{11}
	4	–	67.11	–	–	32.79	0.03	–	0.07	β-Mg_2Si
FSP at 1200 rpm	5	23.14	61.98	1.78	12.64	0.25	0.21	–	–	T-$(AlZn)_{49}Mg_{32}$
	6	91.47	4.61	0.58	3.23	–	–	–	0.11	T′-$AlMg_2Zn$
	7	34.21	–	65.34	–	0.14	–	–	0.31	θ-Al_2Cu
FSP at 1600 rpm	8	–	5.97	1.09	92.94	–	–	–	–	η'-Mg_2Zn_{11}
	9	71.15	11.83	15.06	1.86	0.06	–	–	0.04	S′-Al_6CuMg_4

1600 rpm. As summarized in Table 2, the as-received alloy contains two kinds of intermetallic phases with different compositions. A coarse particle with a length of 34 μm and thickness of 18 μm (spot 1) has a chem-

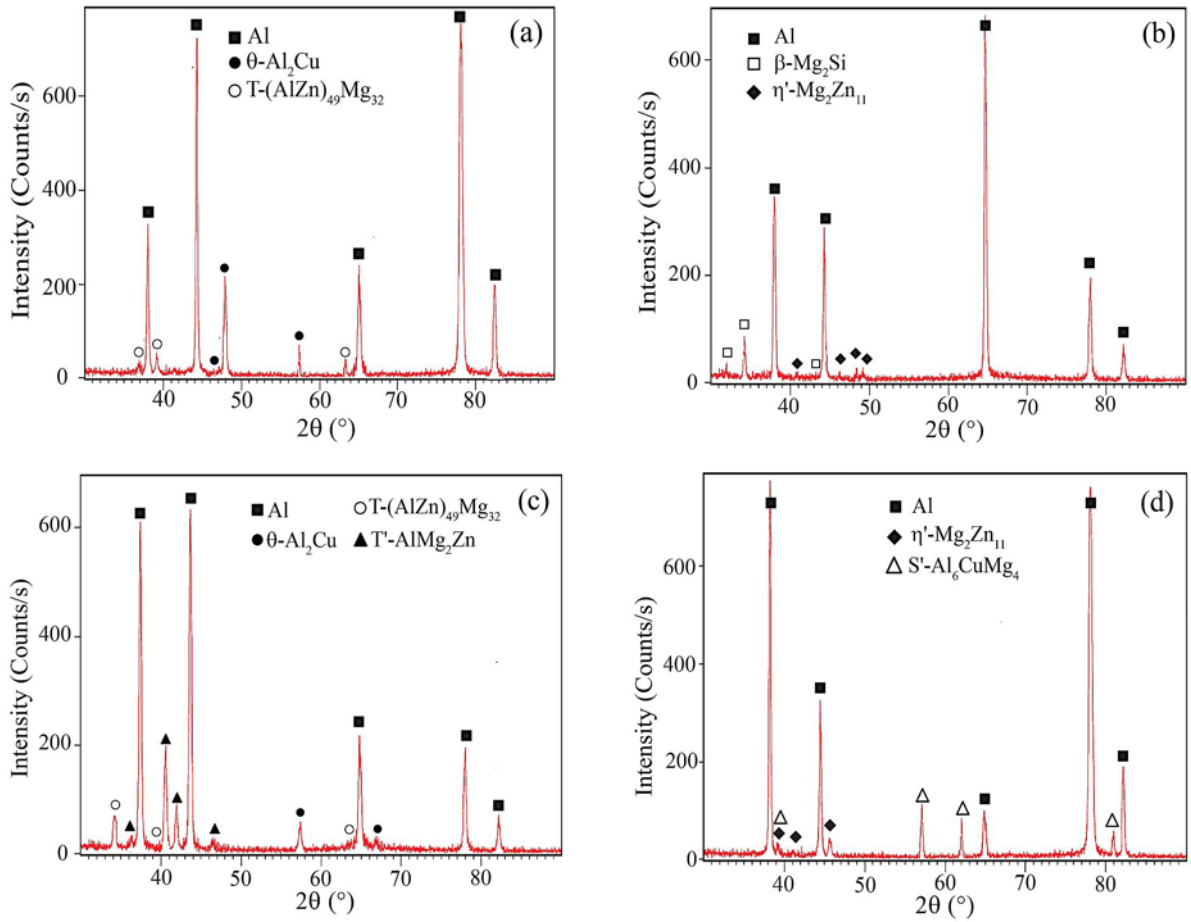

Fig. 7. XRD patterns of the AA 7050 alloy: (a) unprocessed, (b) processed at 800 rpm, (c) processed at 1200 rpm, and (d) processed at 1600 rpm.

ical composition close to the stable T-$(AlZn)_{49}Mg_{32}$ phase. The second intermetallic phase (spot 2) has a needle-shaped form with a length of 3.3 μm and a thickness of 1.8 μm (spot 2). Based on the EDS analysis, this phase is enriched with Cu element, and its stoichiometry is close to that of the θ-Al_2Cu phase. The presence of different intermetallic phases in the unprocessed sample is a consequence of its manufacturing process history.

FSP at 800 rpm led to the development of different intermetallic phases than the unprocessed sample, as shown in Fig. 6b and Table 2. The stoichiometry of the first phase (spot 3) is close to the metastable η'-Mg_2Zn_{11} phase, while the second phase (spot 4) belongs to the β-Mg_2Si phase. Both phases have dimensions of a length of 2.4–3 μm and a thickness of 1–1.2 μm. Figure 6c and Table 2 demonstrated that the sample processed at 120 rpm contains the same phases already present in the unprocessed sample, T-$(AlZn)_{49}Mg_{32}$ phase in spot 5 and θ-Al_2Cu phase in spot 7. Besides, the chemical elements in spot 6 suggest the formation of the metastable T′-$AlMg_2Zn$ phase. It is interesting to note that the sizes of the stable T-$(AlZn)_{49}Mg_{32}$ phase are visibly smaller (3.7 μm in length and thickness of 2 μm) than those present in the unprocessed sample (Fig. 6a), which indicates their fragmentation during the stirring. The SEM in Fig. 6d shows the microstructure of the processed sample at 1600 rpm. The EDS analysis of spots 8 and 9 reveals the development of different intermetallic phases than in the unprocessed and other processed samples. As mentioned in Table 2, the chemical compositions of spots 8 and 9 are close to the metastable η'-Mg_2Zn_{11} and S′-Al_6CuMg_4 phases, respectively. It is apparent that the metastable η'-Mg_2Zn_{11} phase has a small rod-like form with a diameter of 1 μm while the metastable S′-Al_6CuMg_4 phase appears as needle-shaped particles with a length of 2.6 μm and a thickness of 0.8 μm.

Figure 7 shows the XRD patterns of the unprocessed sample and the stir zones of the AA 7050 aluminum alloy under different tool rotational speed conditions. As can be noticed, the XRD patterns confirm the presence of different phases in the samples, and their identifications are in good agreement with the SEM results (Fig. 6 and Table 2). It must be mentioned that the precipitation sequence in the 7xxx al-

loy is complicated and may contain simultaneously different metastable and stable phases such as θ, (η' and η), (T′ and T) phases, or (S′ and S) phases depending on the Cu content and the Zn/Mg ratio [24].

The SEM observations and XRD patterns demonstrated that the nature of intermetallic phases strongly depends on the tool's rotational speed. The heat generated from stirring is certainly not the same at 800, 1200, and 1600 rpm, which causes the dissolution and precipitation of different metastable and stable phases in the processed samples. Indeed, the heat generated during the stirring increases with increasing the tool's rotational speed. It was reported that the stir zone suffers from SPD and heat generation with maximum temperatures in the range of 0.6–0.95 T_m (T_m is the melting temperature) [13]. Unfortunately, the temperature measurement in the stir zone could not be made during the present investigation. Moreover, the generation of dislocations and vacancies during stirring serves as a rapid diffusion path to the solute atoms, accelerating the development of precipitate phases [6].

It was shown in many investigations that increasing the rotational speed and decreasing the travel speed result in high heating generation, which promotes the grain growth of the dynamically recrystallized grains in the stir zone and eventually causes the coarsening of the microstructure [25–27]. However, the present investigation shows completely the opposite behavior. In the present case, the travel speed was kept the same, but the increase in the rotational speed reduced the mean grain size of the stir zone of the present AA 7050 alloy (see Fig. 5). This behavior can be attributed to the development of different intermetallic phases during stirring at different rotational speeds (Figs. 6 and 7, Table 2). Figure 5 shows that the precipitate phases are mostly at grain boundaries. It is well known that the second phase generally prevents the migration of grain boundaries, leading to restricted grain growth. It can, therefore, be concluded that increasing rotational speed produces smaller grain sizes due to the simultaneous occurrence of DRX and the development of precipitate phases. Consequently, the evolution of mechanical properties as a function of rotational speed is discussed in the next section.

3.2. Mechanical properties

The evolution of microhardness in the stir zone along the horizontal and vertical distances of the processed samples at 800, 1200, and 1600 rpm is shown in Fig. 8. The microhardness of the unprocessed alloy was 148 HV, and it is also presented in the plots for comparison.

The microhardness evolution through horizontal and vertical distances exhibits similar behavior in all processed samples. The microhardness value is higher

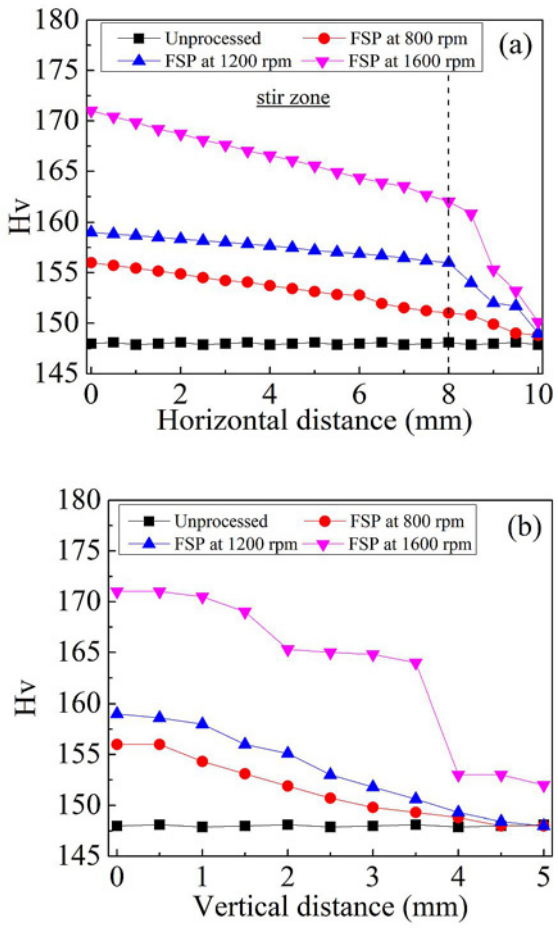

Fig. 8. Evolution of microhardness in the stir zone of the processed samples at 800, 1200, and 1600 rpm: (a) horizontal and (b) vertical distance.

in the center of the stir zone and then decreases with increasing horizontal and vertical distances. It should be mentioned that the decrease in the microhardness of the processed samples from 8 to 10 mm through the horizontal distance (Fig. 8a) does not belong only to the stir zone but to the TMAZ and/or HAZ rather than to the BM. The material in the TMAZ is characterized by a deformed microstructure caused by plastic deformation and insufficient heating for DRX to occur [28]. This explains the minor decrease in the microhardness along the distance from 8 to 9 mm in all processed samples, see Fig. 8a. In contrast, the HAZ is only affected by heat generated during FSP, and its microstructure is usually similar to that of the BM [28]. Hence, the microhardness of HAZ is expected to be similar to that of the BM (148 HV). Concerning the heterogeneity of microhardness distribution through the vertical distance (Fig. 8b), it was expected that the microhardness would be higher at the top surface of the stir zone since the tool shoulder is in direct contact with the top surface of the workpiece, which

Table 3. UTS, YS, yield ratio (YS/UTS), *El*, IS, HV_{max}, mean grain size (d) values, and detected phases of unprocessed and FSP samples at 800, 1200, and 1600 rpm

Condition	UTS (MPa)	YS (MPa)	YS/UTS	*El* (%)	IS (J mm^{-2})	HV_{max} H	d (μm)	Detected phases
Unprocessed	557	471	0.84	8.4	0.51	148	45	T-$(AlZn)_{49}Mg_{32}$ + θ-Al_2Cu
FSP at 800 rpm	576	482	0.83	8.0	0.61	156	28	η'-Mg_2Zn_{11} + β-Mg_2Si
FSP at 1200 rpm	642	465	0.72	6.3	0.56	159	11	T-$(AlZn)_{49}Mg_{32}$ + T′-$AlMg_2Zn$ + θ-Al_2Cu
FSP at 1600 rpm	673	458	0.68	5.8	0.54	171	9	η'-Mg_2Zn_{11} + S′-Al_6CuMg_4

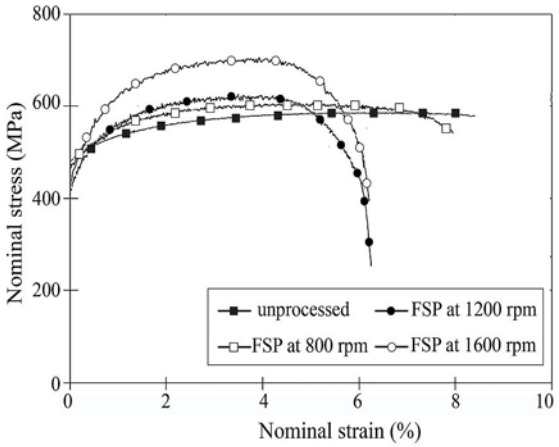

Fig. 9. Nominal stress-strain curves of the unprocessed AA 7050 sample and after FSP at 800, 1200, and 1600 rpm.

brings an additional strain at the top of the stir zone.

The maximum microhardness value of the sample processed at 800 rpm was found to be 156 HV at the center of the stir zone, and it decreased slightly through the distance to reach values of 151 and 148 HV at the outside and the bottom of the stir zone, respectively. It can be noticed that the difference between the microhardness values of the sample processed at 1200 and 800 rpm is not high. The microhardness at the center of the stir zone increases slightly to 159 HV after processing at 1200 rpm and then decreases to 156 and 148 HV at the outside and bottom of the stir zone, respectively. A significant increase in microhardness value to 171 HV is found in the center of the stir zone in the sample processed at 1600 rpm. Then, the microhardness decreases to 162 and 152 HV at the outside and bottom of the stir zone, respectively. It is evident that FSP at 1600 rpm provides the best microhardness evolution.

Figure 9 displays the nominal stress-strain curves of the unprocessed 7050 aluminum alloy and after FSP at 800, 1200, and 1600 rpm. Tensile properties such as ultimate tensile strength (UTS), yield stress (YS), yield ratio (YS/UTS), and percentage elongation (*El*%) of the samples are summarized in Table 3. The unprocessed sample exhibits a tensile strength of 557 MPa, yield stress of 471 MPa, and an elongation of 8.4 %. According to the results, the UTS increased from 576 MPa in the sample processed at 800 rpm to 673 MPa in the sample processed at 1600 rpm. A slight improvement in YS can be noted in the sample processed at 800 rpm, which then decreases with further increasing the tool rotational speed. However, the yield ratio decreases with increasing rotational speed (see Table 3), indicating a good resistance performance of the processed samples, especially those processed at high rotational speed (1600 rpm). The elongation depends on the rotational speed, where the elongation continuously decreases from 8.1 % in the unprocessed sample to 5.8 % in the sample processed at 1600 rpm. Thus, the processed samples present low ductility compared to the unprocessed sample. This indicates an increase in the deformation resistance of the processed samples due to the microstructural changes, as noticed earlier in Section 3.1. Table 3 presents the values of the impact strength test for all samples. The impact strength reflects the amount of energy absorbed in the fracture and determines the impact toughness of the sample. As can be noticed, all the processed samples have a slightly higher impact strength than the unprocessed sample. At the same time, an increase in the tool rotational speed causes a reduction in the impact strength (IS) from 0.61 J mm^{-2} at 800 rpm to 0.54 J mm^{-2} at 1600 rpm. It is apparent that impact strength and yield stress share the same behavior.

The variation in mechanical properties of the AA7050 alloy is the direct consequence of the microstructural variation during FPS. The maximum microhardness, mean grain size, and detected precipitate phases in all samples are presented in Table 3 to determine whether there is any correlation between the mechanical properties and the corresponding microstructural evolutions. As can be noticed, the increase in tensile strength and microhardness values and the lowing in the yield ratio and IS values when the rotational speed increases can be directly associated with the decrease in mean grain size and the precipitation of metastable phases such as η'-Mg_2Zn_{11} at 800 rpm, T′-$AlMg_2Zn$ at 1200 rpm, and η'-Mg_2Zn_{11} and S′-Al_6CuMg_4 at 1600 rpm.

Hence, it can be concluded that the FSP at

1600 rpm is the best rotational tool parameter for optimizing the mechanical properties of the AA7050 alloy owing to the small grain size (9 μm) and the precipitation of metastable η'-Mg_2Zn_{11} and S′-Al_6CuMg_4 phases.

4. Conclusions

The surface of the AA 7075 alloy was modified by friction stir processing. Three tool rotational speeds, 800, 1200, and 1600 rpm, were used to evaluate their influence on the microstructural characteristics and the mechanical performance of the processed alloy. The main findings can be drawn as follows:

– AA7050 alloy can be successfully processed by friction stir processing with tool rotational speeds ranging from 800 to 1600 rpm.

– The surface quality of the FSP sample is improved with increased rotational speed.

– FSP resulted in fragmentation of initial phases (T-$(AlZn)_{49}Mg_{32}$ and θ-Al_2Cu) and precipitation of several metastable phases, including η'-Mg_2Zn_{11} at 800 rpm, T′-$AlMg_2Zn$ at 1200 rpm, and η'-Mg_2Zn_{11} and S′-Al_6CuMg_4 at 1600 rpm.

– The mean grain size of the stir zone decreased with increasing the tool rotational speed from 45 μm in the initial state to 9 μm after FSP at 1600 rpm.

– The microhardness value of all processed samples was higher in the center of the stir zone and then decreased with increasing horizontal and vertical distances.

– The mechanical properties of the AA7050 alloy were enhanced by friction stir processing due to the combination of grain refinement and precipitation strengthening.

– The optimum microstructure and mechanical properties were obtained for the sample processed at a rotational speed of 1600 rpm.

References

[1] W. Zhang, J. Xu, Advanced lightweight materials for automobiles: A review, Mater. Des. 221 (2022) 110994. https://doi.org/10.1016/j.matdes.2022.110994

[2] J. V. Christy, A. H. Ismail Mourad, M. M. Sherif, B. Shivamurthy, Review of recent trends in friction stir welding process of aluminum alloys and aluminum metal matrix composites, T. Nonferr. Metal. Soc. 31 (2021) 3281–3309. https://doi.org/10.1016/S1003-6326(21)65730-8

[3] E. O. Hall, The deformation and ageing of mild steel: III. Discussion of results, Proc. Phys. Soc. B 64 (1951) 747–753. https://doi.org/10.1088/0370-1301/64/9/303

[4] N. J. Petch, The cleavage strength of polycrystals, J. Iron Steel Inst. 174 (1953) 25–28.

[5] R. Z. Valiev, Y. Estrin, Z. Horita, T. G. Langdon, M. J. Zehetbauer, Y. T. Zhu, Producing bulk ultrafine-grained materials by severe plastic deformation, JOM 58 (2006) 33–39. https://doi.org/10.1007/s11837-006-0213-7

[6] G. Sha, Y. B. Wang, X. Z. Liao, Z. C. Duan, S. P. Ringer, T. G. Langdon, Influence of equal-channel angular pressing on precipitation in an Al–Zn–Mg–Cu alloy, Acta Mater. 57 (2009) 3123–3132. https://doi.org/10.1016/j.actamat.2009.03.017

[7] H. Azzeddine, B. Mehdi, L. Hennet, D. Thiaudière, B. Alili, M. Kawasaki, D. Bradai, T. G. Langdon, An in situ synchrotron X-ray diffraction study of precipitation kinetics in a severely deformed Cu-Ni-Si alloy, Mater. Sci. Eng. A 597 (2014) 288–294. https://doi.org/10.1016/j.msea.2013.12.092

[8] R. Z. Valiev, T. G. Langdon, Principles of equal-channel angular pressing as a processing tool for grain refinement, Prog. Mater. Sci. 51 (2006) 881–981. https://doi.org/10.1016/j.pmatsci.2006.02.003

[9] Y. Saito, N. Tsuji, H. Utsunomiya, T. Sakai, R. G. Hong, Ultra-fine grained bulk aluminum produced by accumulative roll-bonding (ARB) process, Scr. Mater. 39 (1998) 1221–1227. https://doi.org/10.1016/S1359-6462(98)00302-9

[10] A. P. Zhilyaev, T. G. Langdon, Using high-pressure torsion for metal processing: Fundamentals and applications, Prog. Mater. Sci. 53 (2008) 893–979. https://doi.org/10.1016/j.pmatsci.2008.03.002

[11] R. S. Mishra, Z. Y. Ma, I. Charit, Friction stir processing: A novel technique for fabrication of surface composite, Mater. Sci. Eng. A 341 (2003) 307–310. https://doi.org/10.1016/S0921-5093(02)00199-5

[12] B. T. Gibson, D. H. Lammlein, T. J. Prater, W. R. Longhurst, C. D. Cox, M. C. Ballun, K. J. Dharmaraj, G. E. Cook, A. M. Strauss, Friction stir welding: Process, automation, and control, J. Manufact. Process. 16 (2014) 56–73. https://doi.org/10.1016/j.jmapro.2013.04.002

[13] V. Patel, W. Li, A. Vairis, V. Badheka, Recent development in friction stir processing as a solid-state grain refinement technique: Microstructural evolution and property enhancement, Crit. Rev. Solid State Mater. Sci. 44 (2019) 378–426. https://doi.org/10.1080/10408436.2018.1490251

[14] A. Suri, A. Sahai, K. H. Raj, N. K. Gupta, Impact and tensile testing of Al2024 alloy processed by friction stir processing, Procedia Eng. 173 (2017) 679–685. https://doi.org/10.1016/j.proeng.2016.12.145

[15] W. Yang, H. Ding, Y. Mu, J. Li, W. Zhang, Achieving high strength and ductility in double-sided friction stir processing 7050-T7451 aluminum alloy, Mater. Sci. Eng. A 707 (2017) 193–198. https://doi.org/10.1016/j.msea.2017.09.028

[16] R. S. Mishra, M. W. Mahoney, S. X. McFadden, N. A. Mara, A. K. Mukherjee, High strain rate superplasticity in a friction stir processed 7075 Al alloy, Scr. Mater. 42 (2000) 163–168. https://doi.org/10.1016/S1359-6462(99)00329-2

[17] S. Gholami, E. Emadoddin, M. Talally, E. Borhani, Friction stir processing of 7075 Al alloy and subsequent aging treatment, T. Nonferr. Metal Soc. 25 (2015) 2847–2855. https://doi.org/10.1016/S1003-6326(15)63910-3

[18] V. Patel, V. Badheka, W. Li, S. Akkireddy, Hybrid friction stir processing with active cooling approach to enhance superplastic behavior of AA7075 aluminum alloy, Arch. Civ. Mech. Eng. 19 (2019) 1368–1380. https://doi.org/10.1016/j.acme.2019.08.007

[19] Z. Y. Ma, R. S. Mishra, F. C. Liu, Superplastic behavior of micro regions in two-pass friction stir processed 7075Al alloy, Mater. Sci. Eng. A 505 (2009) 70–78. https://doi.org/10.1016/j.msea.2008.11.016

[20] M. Regev, S. Spigarelli, Study of mechanical, microstructural and thermal stability properties of friction stir processed aluminum 2024-T3 alloy, Kovove Mater. 57 (2019) 229–236. https://doi.org/10.4149/km_2019_4_229

[21] S. Sun, P. Liu, L. Chen, M. Cao, J. Hu, S. Liu, X. Qiao, J. Sun, Micro-nano structure and characterization in the nugget zone of Al-Cu-Mg alloy under friction stir processing, Kovove Mater. 57 (2019) 27–31. https://doi.org/10.4149/km_2019_1_27

[22] H. Fotoohi, B. Lotfi, Z. Sadeghian, J.-W. Byeon, Effect of post-processing heat treatment on microstructure evolution and mechanical properties of in-situ Al/(Al_3Ni-TiC) hybrid composite fabricated by friction stir processing using mechanically activated powders, Kovove Mater. 58 (2020) 211–222. https://doi.org/10.4149/km_2020_3_211

[23] A. L. Helbert, S. Bozzi, T. Baudin, Dynamic recrystallization in similar 5182 Al/Al and dissimilar Al/Fe friction stir spot welds, Materials Science Forum 715–716 (2012) 152–157. https://doi.org/10.4028/www.scientific.net/MSF.715-716.152.

[24] Y. Dai, L. Yan, J. Hao, Review on micro-alloying and preparation method of 7xxx series aluminum alloys: Progresses and prospects, Materials 15 (2022) 1216. https://doi.org/10.3390/ma15031216

[25] V. V. Patel, V. J. Badheka, A. Kumar, Effect of velocity index on grain size of friction stir processed Al-Zn-Mg-Cu alloy, Proc. Technol. 23 (2016) 537–542. https://doi.org/10.1016/j.protcy.2016.03.060

[26] M. Mosallaee, M. Dehghan, Improvement of structural and mechanical properties of Al-1100 alloy via friction stir processing, J. Mater. Eng. Perform. 23 (2014) 3786–3793. https://doi.org/10.1007/s11665-014-1155-9

[27] L. Karthikeyan, V. S. Senthilkumar, V. Balasubramanian, S. Natarajan, Mechanical property and microstructural changes during friction stir processing of cast aluminum 2285 alloy, Mater. Des. 30 (2009) 2237–2242. https://doi.org/10.1016/j.matdes.2008.09.006

[28] T. Baudin, S. Bozzi, F. Brisset, H. Azzeddine, Local microstructure and texture development during friction stir spot of 5182 aluminum alloy, Crystals 13 (2023) 540. https://doi.org/10.3390/cryst13030540